1 h-channels contribute to divergent electrophysiological properties of

2 supragranular pyramidal neurons in human versus mouse cerebral cortex

- 3
- 4 Brian E Kalmbach<sup>1,2</sup>\*, Anatoly Buchin<sup>1</sup>, Jeremy A Miller<sup>1</sup>, Trygve E Bakken<sup>1</sup>,
- 5 Rebecca D Hodge<sup>1</sup>, Peter Chong<sup>1</sup>, Rebecca de Frates<sup>1</sup>, Kael Dai<sup>1</sup>, Ryder P.
- 6 Gwinn<sup>3</sup>, Charles Cobbs<sup>4</sup>, Andrew L Ko<sup>5,6</sup>, Jeffrey G Ojemann<sup>5,6</sup>, Daniel L
- 7 Silbergeld<sup>6</sup> Christof Koch<sup>1</sup>, Costas A. Anastassiou<sup>1,7</sup>, Ed Lein<sup>1, 6</sup>, Jonathan T
- 8 Ting<sup>1</sup>\*
- 9
- <sup>1</sup> Allen Institute for Brain Science, Seattle, WA;
- <sup>2</sup> Department of Physiology and Biophysics, University of Washington, Seattle,
- 12 WA
- <sup>3</sup> Epilepsy Surgery and Functional Neurosurgery, Swedish Neuroscience
- 14 Institute, Seattle, WA;
- <sup>4</sup> The Ben and Catherine Ivy Center for Advanced Brain Tumor Treatment,
- 16 Swedish Neuroscience Institute, Seattle, WA;
- <sup>17</sup> <sup>5</sup> Regional Epilepsy Center at Harborview Medical Center, Seattle, WA;
- <sup>6</sup> Department of Neurological Surgery, University of Washington School of
- 19 Medicine, Seattle, WA;
- <sup>7</sup> Department of Neurology, University of British Columbia, Vancouver, BC
- 21 \*Correspondence: <u>briank@alleninstitute.org</u>, jonathant@alleninstitute.org
- 22

23	Summary			
24 25	Gene expression studies suggest that differential ion channel expression			
26	contributes to differences in rodent versus human neuronal physiology. We			
27	tested whether h-channels more prominently contribute to the physiological			
28	properties of human compared to mouse supragranular pyramidal neurons.			
29	Single cell/nucleus RNA sequencing revealed ubiquitous HCN1-subunit			
30	expression in excitatory neurons in human, but not mouse supragranular layers.			
31	Using patch-clamp recordings, we found stronger h-channel-related membrane			
32	2 properties in supragranular pyramidal neurons in human temporal cortex,			
33	compared to mouse supragranular pyramidal neurons in temporal association			
34	area. The magnitude of these differences depended upon cortical depth and was			
35	largest in pyramidal neurons in deep L3. Additionally, pharmacologically blocking			
36	h-channels produced a larger change in membrane properties in human			
37	compared to mouse neurons. Finally, using biophysical modeling, we provided			
38	evidence that h-channels promote the transfer of theta frequencies from dendrite-			
39	to-soma in human L3 pyramidal neurons. Thus, h-channels contribute to			
40	between-species differences in a fundamental neuronal property.			
41				

bioRxiv preprint doi: https://doi.org/10.1101/312298; this version posted May 2, 2018. The copyright holder for this preprint (which was not certified by peer review) is the author/funder. All rights reserved. No reuse allowed without permission.

42

### Introduction

43	The development and gross anatomical organization of the mammalian			
44	cerebral cortex is stereotyped across species (Angevine and Sidman, 1961;			
45	DeFelipe, 2011; Rakic, 1974). However, while all mammals possess a			
46	hexalaminar cortex comprising diverse neuronal cell types, the primate cortex			
47	has undergone dramatic evolutionary expansion, especially in layers (L) 2 and 3			
48	(DeFelipe, 2011). Consequently, in contrast to rodent, L2 and 3 in human			
49	neocortex are easily distinguishable from each other and further sublaminar			
50	distinctions within layer 3 can be made based upon the size and organization of			
51	pyramidal neurons (DeFelipe, 2011; von Economo and Koskinas, 2007; Hill and			
52	Walsh, 2005; Molnár et al., 2014; Rakic, 2009). This evolutionary expansion and			
53	stratification suggests that there is functional specialization of neuronal properties			
54	within the supragranular layers of human neocortex.			
55	Cross-species comparisons of supragranular pyramidal neuron properties			
56	indeed suggest that such neuronal specializations exist. For example,			
57	supragranular pyramidal neurons are larger and display more complex dendritic			
58	branching in human compared to the mouse (Deitcher et al., 2017; Mohan et al.,			
59	2015). Additionally, there appear to be differences in the passive membrane			
60	properties of human neurons that may compensate for the filtering of electrical			
61	signals that would occur along such extensive dendritic arbors (Eyal et al., 2016).			
62	These differences may contribute to the unique cable properties of human			
63	pyramidal neuron dendrites and the enhanced ability of human neurons to track			
64	high frequency synaptic input (Eyal et al., 2014; Testa-Silva et al., 2014).			

65	While these differences in passive neuronal properties are notable,				
66	surprisingly little is known about how differential ion channel expression				
67	contributes to differences in active membrane properties between human versus				
68	rodent neurons. Voltage-gated ion channels shape a neuron's subthreshold				
69	integrative properties and endow it with the ability to generate non-linear,				
70	regenerative events, including axonal action potentials and dendritic spikes				
71	(Bean, 2007; Johnston and Narayanan, 2008; Koch, 2004; Reyes, 2001; Stuart				
72	and Spruston, 2015). In this way, ion channels are prime contributors to				
73	specialized neuronal function. Intriguingly, large-scale cross-species				
74	comparisons of gene expression have revealed differences in the laminar				
75	expression of several ion channel-associated genes between mouse and humar				
76	cortex (Zeng et al., 2012). Specifically, RNA for HCN1, a major pore-forming				
77	subunit of h-channels (Robinson and Siegelbaum, 2003) is differentially				
78	expressed in human versus mouse neocortex (Zeng et al., 2012). The				
79	hyperpolarization-activated non-specific cation current, $I_h$ , which is carried by h-				
80	channels, greatly shapes a neuron's subthreshold integrative properties (Magee,				
81	1998; Robinson and Siegelbaum, 2003; Williams and Stuart, 2000).				
82	Here, we use single nucleus transcriptomics and in vitro slice physiology				
83	to provide evidence that h-channels contribute to the membrane properties of				
84	supragranular pyramidal neurons in human cortex more so than in mouse cortex.				
85	We then use a biophysical model to provide insight into how the presence of h-				
86	channels affects the integrative properties of human supragranular pyramidal				
87	neurons. Our findings implicate a species-specific role for h-channels in dendritic				

88	integration of	synaptic inp	ut that is most	pronounced in o	deep L3 pyramida	al
----	----------------	--------------	-----------------	-----------------	------------------	----

- neurons of human temporal cortex, which may generally represent an important
- 90 evolutionary adaptation for very large pyramidal neurons in the human neocortex.
- 91 Experimental Procedures

#### 92 Human surgical specimens

93 Surgical specimens were obtained from local hospitals (Harborview Medical

- 94 Center, Swedish Medical Center and University of Washington Medical Center)
- 95 in collaboration with local neurosurgeons. All patients provided informed consent
- 96 and experimental procedures were approved by hospital institute review boards
- 97 before commencing the study. The bulk of data included in this study were
- 98 obtained from tissue from 10 patients with temporal lobe epilepsy with a mean
- age of 38.10 ± 15.67. Four patients were male and 6 were female. Additionally,
- 100 data were obtained from tissue from one patient who had undergone deep tumor
- 101 resection from the temporal lobe. Tissue obtained from surgery was distal to the

102 core pathological tissue and was deemed not to be of diagnostic value.

103 Specimens were placed in a sterile container filled with an artificial cerebral

spinal fluid (aCSF) composed of (in mM): 92 with N-methyl-D-glucamine

105 (NMDG), 2.5 KCl, 1.25 NaH<sub>2</sub>PO<sub>4</sub>, 30 NaHCO<sub>3</sub>, 20 4-(2-hydroxyethyl)-1-

106 piperazineethanesulfonic acid (HEPES), 25 glucose, 2 thiourea, 5 Na-ascorbate,

- 107 3 Na-pyruvate, 0.5 CaCl<sub>2</sub>·4H<sub>2</sub>O and 10 MgSO<sub>4</sub>·7H<sub>2</sub>O. The pH of the NMDG
- 108 aCSF was titrated to pH 7.3–7.4 with concentrated hydrochloric acid and the
- 109 osmolality was 300-305 mOsmoles/Kg. The solution was pre-chilled to 2-4°C
- and thoroughly bubbled with carbogen  $(95\% O_2/5\% CO_2)$  prior to collection.

111 Surgical specimens were quickly transported from the surgical site to the

112 laboratory while continuously bubbled with carbogen (transportation time: 10-40

113 minutes).

114 Acute brain slice preparation

115 To ensure that the dendrites of pyramidal neurons were relatively intact, 116 human surgical specimens were trimmed and mounted such that the angle of 117 slicing was perpendicular to the pial surface. 350 µm thick slices were sectioned 118 on a Compresstome VF-200 (Precisionary Instruments) using the NMDG 119 protective recovery method (Ting et al., 2014) and either a zirconium ceramic 120 blade (EF-INZ10, Cadence) or a sapphire knife (93060, Electron Microscopy 121 Sciences). The slicing solution was the same as used for transport from the 122 hospital to the laboratory. After all sections were obtained, slices were 123 transferred to a warmed (32-34° C) initial recovery chamber filled with NMDG 124 aCSF under constant carbogenation. After 12 minutes, slices were transferred to 125 a Brain Slice Keeper-4 holding chamber (Automate Scientific) containing an 126 aCSF solution made of (in mM): 92 NaCl, 2.5 KCl, 1.25 NaH<sub>2</sub>PO<sub>4</sub>, 30 NaHCO<sub>3</sub>, 127 20 HEPES, 25 glucose, 2 thiourea, 5 Na-ascorbate, 3 Na-pyruvate, 2 128 CaCl<sub>2</sub> 4H<sub>2</sub>O and 2 MgSO<sub>4</sub> 7H<sub>2</sub>O continuously bubbled with 95/5 O<sub>2</sub>/CO<sub>2</sub>. Slices 129 were held in this chamber at room temperature for 1-48 hours before transfer to 130 the recording chamber for patch clamp recording. 131 All procedures involving mice were approved by the Institutional Animal

132 Care and Use Committee. Mouse brain slices were prepared in largely the same 133 fashion as human slices. Four male and 6 female mice, 44-61 days old (49.8 ±

5.59), were deeply anesthetized by intraperitoneal administration of Advertin (20
mg/kg IP) and were perfused through the heart with NMDG aCSF (bubbled with
carbogen). Coronal slices containing the temporal association area (TeA) were
prepared as described for human with the exception that slices were 300 µm
rather than 350 µm thick.

139 Patch clamp recordings

140 Slices were placed in a submerged, heated (32-34° C) recording chamber

141 that was continually perfused (3-4 mL/min) with aCSF under constant

142 carbogenation and containing the following (in mM): 119 NaCl, 2.5 KCl, 1.25

143 NaH<sub>2</sub>PO<sub>4</sub>, 24 NaHCO<sub>3</sub>, 12.5 glucose, 2 CaCl<sub>2</sub>·4H<sub>2</sub>O and 2 MgSO<sub>4</sub>·7H<sub>2</sub>O (pH 7.3-

144 7.4). Slices were viewed with an Olympus BX51WI microscope and infrared

145 differential interference contrast optics and a 40x water immersion objective.

146 Patch pipettes (3-6 MΩ) were pulled from borosilicate glass using a horizontal

147 pipette puller (P1000, Sutter Instruments). The pipette solution for all

experiments contained the following (in mM): 130 K-gluconate, 10 HEPES, 0.3

149 EGTA, 4 Mg-ATP, 0.3 Na<sub>2</sub>-GTP and 2 MgCl<sub>2</sub>. The pipette solution also contained

150 5% biocytin and 20 µM Alexa 594. These were included to ensure that the apical

151 dendrite reached the pial surface. Alexa filled cells were visualized only upon

152 termination of the recording using a 540/605 nm excitation/emission filter set.

153 The theoretical liquid junction potential was calculated to be -13 mV and was not

154 corrected

155 Whole cell somatic recordings were acquired using a Multiclamp 700B 156 amplifier and PClamp 10 data acquisition software (Molecular Devices). Electrical

157 signals were digitized (Axon Digidata 1550B) at 20-50 kHz and filtered at 2-10 158 kHz. Upon attaining whole-cell current clamp mode, the pipette capacitance was 159 compensated and the bridge was balanced. Access resistance was monitored 160 throughout the recording and was 8-25 MΩ. Recordings were terminated if 161 access resistance exceeded 25 MΩ. ZD7288 (10  $\mu$ M; Tocris) was prepared from 162 frozen concentrated stock solutions and diluted in recording aCSF.

163 Data analysis and statistical testing

164 Data were analyzed using custom analysis scripts written in Igor Pro 165 (Wavemetrics). All measurements were made at resting membrane potential and, 166 in a subset of experiments, at a common potential of -65 mV. Input resistance 167  $(R_N)$  was calculated from the linear portion of the current-voltage relationship 168 generated in response to a series of 1s current injections (-150 to +50 pA, 20 or)169 50 pA steps). The maximum and steady state voltage deflections were used to 170 determine the maximum and steady state of  $R_N$ , respectively. Voltage sag was 171 defined as the ratio of maximum to steady-state R<sub>N</sub>. Rebound slope was 172 calculated from the slope of the rebound amplitude as a function of steady-state 173 membrane potential. Resonance was determined from the voltage response to a 174 constant amplitude sinusoidal current injection that linearly increased in 175 frequency from 1-14 or 15 Hz over 15 s. The impedance amplitude profile (ZAP) 176 was constructed from the ratio of the fast Fourier transform of the voltage 177 response to the fast Fourier transform of the current injection. The frequency 178 corresponding to the peak impedance  $(Z_{max})$  was defined as the resonant 179 frequency. The 3dB cutoff was calculated as the frequency at which the ZAP

profile attenuated to a value of ( $\sqrt{1/2}$ ) Z<sub>max</sub>. Action potentials (APs) were elicited in response to increasing amplitude, 1s direct current injections (50-750 pA, 50 pA steps).

183 Statistical analyses and plotting were performed using Prism (Graphpad).

184 Data are presented in the text as mean ± SEM or R<sup>2</sup> values. Between-subject

185 ANOVA, mixed factors ANOVA, two-sample Kolmogorov-Smirnov test and post

186 hoc t-tests were used to test for statistical differences between groups.

187 Bonferroni correction was used to correct for multiple comparisons. Pearson's

188 product moment correlation was used to test for statistically significant

189 correlations between variables.

190 Biophysical model

191 The morphological reconstruction (Figure 7) was generated using

192 methods previously described (Allen Institute for Brain Science, 2016; Gouwens

193 et al., 2018). Briefly, the tissue slice was stained via diaminobenzidine reaction to

194 elucidate biocytin filled cells. Z-stacks of the cell were imaged at 63x

195 magnification on a Zeiss Axio Imager 2. Reconstruction was manually performed

using Vaa3D software to create accurate full neuron representations of the soma,

dendrites, and axon saved in the SWC format (Peng et al., 2010).

198 The single neuron model was simulated using the Neuron 7.4 simulator

199 (https://www.neuron.yale.edu/neuron/) in combination with the Brain Modeling

200 Toolkit (https://github.com/AllenInstitute/bmtk). The morphology of the simulated

201 neuron was adopted from the SWC file generated in the morphology

202 reconstruction process. The dendritic tree was discretized using 20 µm spatial

203 steps and corresponding cylindrical compartments were generated for all 204 compartments. The model was simulated using temporal steps of 0.1 ms. We 205 insured that further reduction of spatial and temporal discretization steps did not 206 provide quantitatively different results. Passive membrane parameters were 207 adjusted for axonal, somatic, apical and basal dendrites compartments. Leak 208 conductance, capacitance, leak reversal potential and axial resistance were fitted 209 to the subthreshold responses of a human pyramidal neuron in response to the 210 family of somatic current injections used to estimate passive parameters using 211 genetic algorithms from DEAP library (https://github.com/DEAP/deap). The best parameters to fit the subthreshold responses were:  $g_{pas}^{soma} = 1.90 * 10^{-5} S/cm^2$ ; 212  $g_{pas}^{basal} = 4.46 * 10^{-6} \, S/cm^2$ ;  $g_{pas}^{axon} = 0.4 * 10^{-3} \, S/cm^2$ ;  $g_{pas}^{apical} = 0.3 * 10^{-3} \, S/cm^2$ 213  $cm^2$ ;  $g_{pas}^{soma} = 1.9 * 10^{-5} \ S/cm^2$ ;  $V_{leak}^{soma} = -79.65 \ mV$ ;  $V_{leak}^{basal} = -86.67 \ mV$ ; 214  $V_{leak}^{axon} = -68.35 \ mV; \ V_{leak}^{apical} = -84.54 \ mV; \ C_m^{soma} = 2.72 \ \mu F/cm^2; \ C_m^{basal} = -84.54 \ mV; \ MV; \ MV = -68.35 \ mV = -68.35 \ mV; \ MV = -68.35 \ mV = -68.35 \ mV; \ MV = -68.35 \ mV = -68.35 \ mV; \ MV = -68.35 \ mV$ 215 1.81  $\mu F/cm^2$ ;  $C_m^{axon} = 1.75 \ \mu F/cm^2$ ;  $C_m^{apic} = 2.91 \ \mu F/cm^2$ ;  $R_{axial}^{soma} = 304 \ Ohm * cm$ ; 216  $R_{axial}^{basal} = 104.08 \ Ohm * cm; R_{axial}^{axon} = 331.68 \ Ohm * cm; R_{axial}^{apical} = 393.53 \ Ohm * cm.$ 217 218 The kinetic parameters of I<sub>h</sub> were adopted from (Kole et al., 2006) and m<sub>alpha</sub> 219 function was shifted by -20 mV to match the junction potential estimation from the 220 experimental data. I<sub>h</sub> and the corresponding HCN conductance was uniformly 221 distributed in somatic, axonal and dendritic compartments,  $g_{HCN} = 0.01 *$ 222  $10^{-3} S/cm^2$ . The maximal conductance  $(g_{HCN})$  for  $I_h$  was adjusted such that the 223 difference in  $R_N$  between the  $I_h(+)$  and  $I_h(-)$  models matched the difference in  $R_N$ 224 observed in experiments after the blockade of I<sub>h</sub> current by ZD7288. The model

possessed no other active conductances. The model code is available on github
page https://github.com/AllenInstitute/\*\*\*.

227 Synaptic conductances (10 nS) were simulated using AMPA-like kinetics: 228  $T_{rise} = 1.5 \text{ ms}, T_{decav} = 3 \text{ ms}, reversal potential} = 0 \text{ mV}$  (Andrasfalvy and Magee, 229 2001; Jonas and Sakmann, 1992; Spruston et al., 1995). For simulations 230 involving random activation of 1000 synaptic inputs, the synaptic conductance of each synapse was scaled to 0.001 mS/cm<sup>2</sup>. Three random seeds were 231 232 instantiated using Python Numpy to generate temporal permutations of synaptic 233 population activation (total simulation duration: 30 s). All results of simulations 234 were stored in NWB file format. Synapses were activated by a Poisson process 235 with 4 Hz rate generated using Numpy expovariate() function. All simulations 236 were performed on a MacBook Pro Retina with 2.8 GHz Intel core i7processor 237 with 16 GB DDR3 RAM running Mac OS 10.13.3 Sierra.

238

239 Results

240 To gain initial insight into whether human supragranular pyramidal 241 neurons express h-channels, we utilized the existing online Allen Cell Types 242 Database (www.celltypes.brain-map.org; methods are included on website) 243 consisting of single-nucleus RNA sequencing (n=15,928 nuclei) from human 244 postmortem brain specimens. Briefly, this method involved layer dissections of 245 thin Nissl-stained human temporal cortex section, neuronal nuclei staining 246 (NeuN) and Fluorescence-activated cells sorting (FACS) isolation, followed by 247 Smart-seq v4 based library preparation and single-cell deep (2.5 million

248 reads/cell) RNA-Seq. GAD1 and SLC17A7 expression were used to delineate 249 inhibitory and excitatory neurons, respectively. For a comparison, in mouse we 250 analyzed a previously published single cell RNA sequencing dataset obtained 251 from mouse primary visual cortex (Tasic et al., 2016). We examined the 252 expression levels of the four pore forming subunits (HCN1-4) of h-channels as 253 well as *PEX5L* which codes for a protein (Trip8b) involved in modulating h-254 channel function and dendritic enrichment (Lewis et al., 2009; Robinson and 255 Siegelbaum, 2003; Santoro, 2004).

256 In human temporal cortex, HCN1 and PEX5L were prominently expressed 257 in excitatory neurons in the supragranular and infragranular layers, whereas 258 HCN2-4 subunits were much less abundant (Figure 1A). The average expression 259 of *HCN1* was approximately equal (1.1 fold higher) in supragranular compared 260 with infragranular excitatory neurons. In contrast, in the mouse neocortex HCN1 261 and *PEX5L* were abundant in infragranular, but not supragranular excitatory 262 neurons (Figure 1B). The average expression of *HCN1* was 3 fold higher in 263 infragranular compared with supragranular excitatory neurons. Furthermore, 264 HCN2-4 expression was relatively very low in excitatory neurons across the 265 layers. Consistent with these observations, HCN1 expression was observed in 266 the supragranular and infragranular layers of human temporal cortex by ISH 267 (Figure 1C; data obtained from the Allen Brain Atlas, human.brain-map.org), 268 whereas in mouse it was seen most conspicuously in L5 in multiple brain regions, 269 including primary visual cortex and temporal association area (TeA; Figure 1D; 270 data obtained from Allen Brain Atlas, mouse brain-map.org). Notably, HCN1

271 expression was relatively high in interneuron populations in mouse and human

272 cortical tissue (Figures 1A and B), suggesting that the scattered labeling in the

273 supragranular layers of mouse cortex via ISH represent interneurons (Figure 1D).

274 Together these data suggest that there is widespread expression of h-channels,

especially those containing HCN1 subunits, in human, but not mouse,

supragranular pyramidal neurons.

#### 277 Physiological evidence for differences in I<sub>h</sub>

278 To allow for direct between-species comparisons of pyramidal neuron 279 membrane properties as a function of somatic distance from the pial surface, we 280 first examined differences in the gross cytoarchitecture of mouse and human 281 cortex. For these purposes we chose the TeA of mouse cortex because it has 282 been used in previous studies as a comparator for the middle temporal cortex 283 typically resected from human patients (Eyal et al., 2016; Mohan et al., 2015; 284 Testa-Silva, 2010; Wang et al., 2015). We performed DAPI staining on thick 285 (350 µm) sections of mouse temporal association (4 slices from 4 mice) and 286 human temporal (6 slices from 6 patients) cortex (Figure S1A). In both species 287 we observed a sharp increase in cell density marking the boundary between L1 288 and L2 (mouse 151 ± 14 µm, human 276 ± 12 µm from pial surface). Below L2 289 was a sparser region of cells (L3) followed by a tight band of densely packed 290 cells (L3/L4 boundary, mouse 470  $\pm$  6  $\mu$ m, human 1469  $\pm$  34  $\mu$ m from pial 291 surface). Notably, the distance from the pial surface to the L3/L4 border ranged 292 from 1292-1637 µm in human sections and 453-508 µm in mouse sections. L4 293 was followed by a decrease in cell density, marking L5 (mouse 599  $\pm$  10  $\mu$ m from

294 pial surface, human 1736 ± 37 µm from pial surface). Finally, the bottom of L6 295 was 2963  $\pm$  97  $\mu$ m and 1252  $\pm$  29  $\mu$ m from the pial surface in human and mouse 296 neocortex, respectively. Thus, L2/3 represents ~40% and ~25% of the total 297 thickness of human temporal gyrus and mouse TeA, respectively. These 298 observations are consistent with previous reports that illustrate the large 299 expansion of supragranular cortex in the human cortical column relative to 300 mouse (DeFelipe, 2011; von Economo and Koskinas, 2007). 301 We performed whole cell patch clamp recordings from supragranular 302 pyramidal neurons with cell bodies located throughout the entire depth of L2 and 303 L3 (sample biocytin fills in Figures S1B and C; human n=55 cells between 350-304 1600 µm, mouse n=39 cells between 162-465 µm from the pial surface). Using 305 IR-DIC optics, L3 was easily distinguishable from L4 both in terms of cell size 306 and density; deep L3 consisted of sparse, large pyramidal neurons whereas L4

307 consisted of more densely packed granular-appearing cells. Morphological

308 differences between mouse and human supragranular pyramidal neurons have

309 been extensively detailed elsewhere, thus we did not pursue them further

310 (Deitcher et al., 2017; Mohan et al., 2015).

We compared  $I_h$ -related membrane properties in human versus mouse pyramidal neurons. h-channels are open at relatively hyperpolarized potentials and thus contribute to a neuron's input resistance ( $R_N$ ) and resting membrane potential (RMP; Magee, 1998; Robinson and Siegelbaum, 2003). As an initial test for differences in the functional expression of h-channels, we measured the RMP and  $R_N$  of pyramidal neurons throughout the depth of mouse and human

317 supragranular cortex. Sample voltage responses obtained from a superficial and 318 deep supragranular pyramidal neuron from both species are shown in Figures 2A 319 and B. In both mouse and human temporal cortex, we observed a positive 320 correlation between RMP and somatic distance from the pial surface, such that the most depolarized neurons were found deep in L3 (mouse  $r^2 = 0.35$ , p<0.001; 321 human  $r^2$  = 0.19, p<.001; Figures 2C-E). In contrast, the R<sub>N</sub> of mouse neurons 322 323 increased as a function of somatic distance from pial surface (0.34, p<.001; Figures 2C and E) whereas the  $R_N$  of human neurons decreased ( $r^2$ = 0.31. 324 325 p<.001; Figures 2D and E). Thus, in human temporal cortex, the neurons with the 326 lowest input resistance were found deep in L3 whereas in mouse cortex they 327 were found superficially, near the L1/2 border (Figure 2E). For human temporal 328 cortex, these general observations were replicated in a subset of experiments in 329 which  $R_N$  was measured at a common membrane potential of -65 mV (Figure S2; n = 43,  $r^{2=}0.32$ , p < 0.001). In contrast, in mouse there was no correlation 330 331 between R<sub>N</sub> and somatic distance from pia in a subset of experiments performed 332 at -65 mV (Figure S2; n = 24,  $r^{2=0.02}$ , p= 0.53). Notably, the observation that  $R_N$ 333 increases as a function of somatic depth from the pial surface in mouse temporal 334 association cortex is consistent with a previous report from mouse prefrontal 335 cortex (Routh et al., 2017). Thus, the depth-dependence of R<sub>N</sub> observed here 336 might be a hallmark of mouse L2/3 regardless of cortical region.

To make direct comparisons between mouse and human pyramidal neuron properties, we binned the data into quarters based on normalized soma distance from the pial surface to the border of L3 and L4. Human neurons were

340	more depolarized than mouse neurons throughout the first three quarters of				
341	supragranular cortex (p = 0.03; ANOVA followed by post-hoc comparisons;				
342	Figure 2F). Furthermore, human neurons displayed a higher $R_{N}$ in the most				
343	superficial portion of supragranular cortex and lower $R_{N}$ in the lower half of				
344	supragranular cortex (p < 0.001; ANOVA followed by post-hoc comparisons;				
345	Figure 2F). These data demonstrate significant distance-dependent differences				
346	in the properties of human versus mouse supragranular pyramidal neurons.				
347	In addition to contributing to $R_N$ , $I_h$ contributes to several unique				
348	membrane properties. Specifically, $I_h$ is associated with a characteristic voltage				
349	"sag" upon membrane hyperpolarization and a rebound potential upon release				
350	from hyperpolarization (Figures 3A and B). These voltage responses reflect the				
351	activation and deactivation kinetics of h-channels (Robinson and Siegelbaum,				
352	2003). While in the supragranular layers of mouse temporal association area				
353	these $I_h\text{-}related$ membrane properties were largely absent, we did observe a few				
354	neurons deep in L3 that displayed modest amounts of sag and rebound (sag $r^2$ =				
355	0.14, p = 0.02, rebound sag $r^2$ = 0.26, p < 0.001; Figure 3C). In contrast, sag and				
356	rebound were apparent in many human pyramidal neurons throughout the				
357	supragranular layers and were positively correlated with somatic depth from the				
358	pial surface (sag $r^2$ = 0.18, p = 0.001, rebound $r^2$ = 0.20, p < 0.001; Figure 3D).				
359	These response properties are plotted as a function of normalized depth from pia				
360	to the border of L3 and L4 and illustrate the marked differences in $I_{\rm h}\mbox{-}related$				
361	properties between mouse and human supragranular pyramidal neurons (Figure				
362	3E). These general observations were replicated in a subset of experiments				

performed at -65 mV (Figures S2 and S3; mouse n=24, sag  $r^2 = 0.01$ , p = 0.65, rebound  $r^2 = 0.35$ , p = 0.002; human n=43, sag  $r^2 = 0.14$ , p = 0.01, rebound  $r^2 = 0.22$ , p < 0.001). Finally, direct between-species comparisons revealed that human neurons possessed more sag and rebound at all levels of supragranular cortex compared to their mouse counterparts (Figure 3F; p < 0.001; ANOVA followed by post-hoc comparisons).

369 The slow activation and deactivation kinetics of h-channels contribute 370 greatly to the filtering properties of a neuron. Specifically, I<sub>h</sub> contributes to 371 membrane resonance in the ~2-7 Hz range (Dembrow et al., 2010; Hutcheon et 372 al., 1996; Kalmbach et al., 2013; 2017; 2015; Narayanan and Johnston, 2007; 373 Nolan et al., 2004; Ulrich, 2002). To test for differences in the subthreshold 374 filtering properties of human versus mouse pyramidal neurons, we measured the 375 response of pyramidal neurons throughout the depth of supragranular cortex to a 376 chirp stimulus. In addition to measuring the resonant frequency of neurons, we 377 also calculated the 3 dB cutoff as a way to quantify differences in low-pass 378 filtering. Sample voltage responses, ZAPs and normalized frequency response 379 curves for superficial and deep mouse and human neurons are shown in Figures 380 4A and B. Mouse pyramidal neurons were largely non-resonant at either RMP or 381 -65 mV, although there were a few neurons located deep in L3 that showed modest resonance (Figures 4C and S3;  $r^2 = 0.13$ , p = 0.02; -65 mV  $r^2 = 0.01$ , p = 382 383 0.59). Additionally, the 3dB cutoff of mouse neurons was negatively correlated with somatic depth from pia at RMP (Figure 4C,  $r^2 = 0.12$ , p = 0.03), but not at -384 65 mV (Figure S3;  $r^2 = 0.01$ , p = 0.99) indicating that the filtering properties of 385

386 deep supragranular pyramidal neurons were more low-pass than superficial ones 387 at RMP. In contrast, many human pyramidal neurons displayed membrane 388 resonance in the  $\sim$ 2-5 Hz range. Indeed, resonance was positively correlated 389 with somatic depth from pia in human supragranular cortex when measured at RMP (Figure 4D:  $r^2 = 0.13$ . p = 0.007) and -65 mV (Figure S2 1:  $r^2 = 0.32$ . p < 390 391 0.001). In contrast to mouse pyramidal neurons, the 3dB cutoff of human 392 pyramidal neurons was positively correlated with somatic depth from pia (Figure 4D: RMP.  $r^2 = 0.12$ , p = 0.01; Figure S2; -65 mV  $r^2 = 0.22$ , p = 0.001), such that 393 394 the filtering properties of superficial neurons were distinct from deep neurons. 395 The 3 dB cutoff and resonance frequency of mouse and human pyramidal 396 neurons are also plotted as a function of normalized soma position in L2/3 397 (Figure 4E). Direct comparisons revealed that human neurons had a higher 398 resonant frequency than mouse neurons at all relative distances from the pial 399 surface (Figure 4F; p < 0.001; ANOVA). Furthermore, the most superficial 400 human neurons had a lower 3dB cutoff than mouse neurons (Figure 4F; p = 0.01; 401 ANOVA followed by post-hoc t test). These data highlight striking differences in 402 the subthreshold filtering properties of mouse versus human L2/3 pyramidal 403 neurons, further supporting the hypothesis that  $I_h$  is prominent in human, but not 404 in mouse supragranular pyramidal neurons.

In addition to contributing to subthreshold properties,  $I_h$  impacts the action potential output of a neuron in response to suprathreshold current injections by affecting  $R_N$ , RMP and after spike potentials (Brager and Johnston, 2007; Fan et al., 2005; Gu et al., 2005). Specifically, differences in the number of action

409 potentials elicited by a given current injection can reflect differences in  $I_{h}$ . Thus, 410 we also tested for between-species differences in the response of individual 411 pyramidal neurons to 1 s, depolarizing direct current injections (250, 500 and 750 412 pA). In mouse temporal association cortex, excitability (here defined as the 413 number of spikes in response to a given current injection) was positively correlated with soma distance from the pial surface (Figure 5A; 250 pA  $r^2$  = 0.38. 414 p < 0.001, 500 pA  $r^2 = 0.17$ , p = 0.01, 750 pA  $r^2 = 0.12$ , p < 0.03), such that the 415 416 most excitable neurons were located deep in L3. In contrast to mouse cortex. 417 excitability was negatively correlated with somatic distance from the pial surface 418 in human cortex such that the most excitable neurons were located superficially (Figure 5B; 250 pA  $r^2$  = 0.21, p < 0.001, 500 pA  $r^2$  = 0.44, p < 0.001, 750 pA  $r^2$  = 419 420 0.47, p < 0.001). Example sweeps obtained from a superficial (top) and deep 421 supragranular (bottom) mouse and human pyramidal neuron are shown in 422 Figures 5A and B. Figure 5C plots the action potential frequency in response to 423 three different amplitudes of current injection in mouse versus human temporal 424 cortex normalized for the position of the recorded neuron through the depth of 425 L2/3. Direct comparisons also revealed several depth-dependent differences in 426 excitability between mouse and human pyramidal neurons (Figure 5D; ANOVA, 427 p<0.001 followed by post-hoc t-tests). These general observations were 428 replicated in a subset of experiments when the membrane potential was held at a 429 common level via direct current injection (-65 mV, Figure S2 and 3). These data 430 suggest that the depth-dependent intrinsic excitability of mouse and human 431 pyramidal neurons differs dramatically. The most excitable human neurons were

located superficially in supragranular cortex whereas the most excitable mouse
neurons were located in the deepest part of the supragranular layers. While
these results mirror the depth-dependent differences in I<sub>h</sub>-dependent membrane
properties described above, there are likely many contributors to these
differences in excitability.

437 The data presented thus far were collected from tissue obtained from 438 patients with temporal lobe epilepsy. To assess the generality of the between-439 species differences in I<sub>h</sub>-related membrane properties, we also obtained data 440 from temporal lobe tissue from a patient diagnosed with a deep brain tumor. The 441 depth-dependent I<sub>h</sub>-related membrane properties observed in tissue obtained 442 from epilepsy patients were also observed in supragranular cortex from this 443 tumor patient (Figure S4). While we can't rule out subtle differences, these data 444 suggest that I<sub>h</sub>-related membrane properties in supragranular pyramidal neurons 445 are not solely related to epilepsy.

# 446 Pharmacological evidence for I<sub>h</sub> in human supragranular pyramidal

447 neurons

448To test for the relative contribution of  $I_h$  to the intrinsic membrane449properties of human versus mouse pyramidal neurons, we bath applied the h-450channel blocker ZD7288 while monitoring resting membrane potential (Figure 6).451For these experiments, we focused on recording from neurons located deeper in452supragranular cortex, where  $I_h$ -related properties were more apparent in both453species. On average, ZD7288 produced a hyperpolarization of the RMP by 9.44454 $\pm$  0.80 mV in human neurons and -0.19  $\pm$  1.68 mV in mouse neurons (Figure 6A).

455 In addition, input resistance, when measured at a common potential of -65 mV 456 increased by 62.14  $\pm$  11.81% in human neurons (from 40.30  $\pm$  2.37 M $\Omega$  to 64.35 457  $\pm 3.23$  M $\Omega$ ) and by 19.47  $\pm 7.89\%$  percent in mouse neurons (from 130.63  $\pm 5.74$ 458 M $\Omega$  to 158.20 ± 11.86 M $\Omega$ ; Figure 6B). ZD7288 also eliminated voltage sag. 459 rebound and resonance, indicating that these membrane properties are 460 dependent on functional h-channels in human supragranular pyramidal neurons 461 (Figure S5). In addition, ZD7288 reduced the cutoff frequency of human neurons more so than mouse (Figure S5). Finally, ZD7288 increased the excitability of 462 463 human pyramidal neurons, as is apparent in the parallel shift of the average 464 input/output curve in Figure 6C. Together, these data suggest that  $I_{\rm h}$  contributes 465 to the intrinsic membrane properties of human supragranular pyramidal neurons 466 significantly more so than mouse neurons.

#### 467 Impact of I<sub>h</sub> on subthreshold integration in human neurons

468 What influence might I<sub>h</sub> have on the input/output properties of human 469 supragranular pyramidal neurons? While I<sub>h</sub> affects many aspects of neuronal 470 function, perhaps its most consistently observed influence is on subthreshold 471 synaptic integration. h-channel expression in many neurons counteracts the 472 distance-dependent capacitive filtering of synaptic input as it propagates from 473 dendrite to soma (Dembrow et al., 2015; Harnett et al., 2015; Koch et al., 1990; 474 Magee, 1999; Magee and Cook, 2000; Rall, 1967; Stuart and Spruston, 1998; 475 Vaidya and Johnston, 2013; Williams and Stuart, 2000); this ensures that the 476 kinetics of synaptic potentials at the soma are relatively independent of synaptic 477 origin. Additionally,  $I_h$  narrows the window for temporal integration of synaptic

478 input often to synaptic inputs with frequency components in the theta (4-12) band 479 (Das and Narayanan, 2014; Dembrow et al., 2015; Kalmbach et al., 2017; 480 Narayanan and Johnston, 2008; 2007; Ulrich, 2002; Vaidya and Johnston, 2013). 481 To explore whether  $I_{\rm h}$  might similarly affect the integrative properties of human 482 supragranular pyramidal neurons, we used a morphologically precise 483 (morphology is shown in Figure 7C) computational model of a human layer 3 484 pyramidal neuron (Methods) that possessed no active conductances other than 485  $I_{h}$ . We chose to model a deep L3 pyramidal neuron where  $I_{h}$ -related properties 486 were more apparent.

487 We first asked whether the presence of I<sub>h</sub> in the model reproduced the 488 subthreshold resonance observed in many deep supragranular pyramidal 489 neurons in human temporal cortex (Figures 7A and B). The presence of  $I_h$ 490 significantly affected the response of the model to a somatic chirp current 491 injection. Notably, even though the chirp stimulus was not used to generate the 492 computational model, in the presence of  $I_h$  (model:  $I_h$  (+)), the model displayed 493 band pass filtering properties closely resembling those observed experimentally 494 (Figures 7A and B). In contrast, in the absence of  $I_h$  (model:  $I_h$  (-)) the frequency 495 response of the model markedly departed from the experimentally measured one 496 (Figures 7A and B).

We next assessed how the presence of I<sub>h</sub> in the model affected the integration of synaptic input arriving at various locations along the dendrite. To this end, we activated AMPA-like conductances at several locations along the dendritic arbor and measured the resultant local dendritic and propagated

501 somatic voltage responses (Figures 7C and D). In a totally passive neuron, low-502 pass filtering severely attenuates and distorts synaptic inputs as they propagate 503 to the soma, especially those arriving at distal locations (Koch, 2004; Koch et al., 504 1990; Rall, 1967; Stuart and Spruston, 1998). To quantify the effect of I<sub>h</sub> on 505 single EPSP kinetics, we measured the delay in the peak of the somatic EPSP 506 relative to the peak of the local dendritic EPSP as well as the halfwidth of the 507 somatic EPSP. In the passive model  $(I_h(-))$  a distance-dependent increase in the 508 delay of the somatic EPSP relative to the dendritic synaptic conductance was 509 observed as well as in the halfwidth of the somatic EPSP. In comparison, in the 510  $I_{h}(+)$  model the delay between the peak of the dendritic and somatic EPSPs was 511 significantly reduced, especially at distal locations, as was the halfwidth of the 512 somatic EPSP (Figures 7E and F). Thus, the inclusion of I<sub>h</sub> produced EPSPs at 513 the soma of the model layer 3 human pyramidal neuron with a significantly faster 514 time course.

515 These effects suggest that I<sub>h</sub> influences the temporal summation of 516 synaptic input in human supragranular pyramidal neurons; faster EPSP kinetics 517 modestly reduce the temporal window wherein inputs can summate (Dembrow et 518 al., 2015; Magee, 1999; Vaidya and Johnston, 2013; Williams and Stuart, 2000). 519 To examine this possibility, we initiated bursts of AMPA-like conductances at 520 various frequencies and different locations along the dendrite and measured the 521 resulting somatic response. The total somatic depolarization (as quantified by 522 the integral of the somatic voltage response) was reduced across several

523 frequencies of synaptic input (Figure 7G). Thus, the presence of I<sub>h</sub> in the model 524 L3 human pyramidal neuron reduced the temporal summation of synaptic inputs. 525 Finally, by opposing changes to membrane potential,  $I_{\rm h}$  can impart 526 phenomenological inductance to the membrane. This has the effect of 527 counteracting lags in the phase of membrane potential relative to current that is 528 imposed by capacitive elements of the membrane (Koch, 1984; Mauro, 1961). 529 This inductive property of I<sub>h</sub> is also known to promote the transfer to the soma of 530 synaptic input containing of theta frequencies (Cook et al., 2007; Dembrow et al., 531 2015; Narayanan and Johnston, 2008; Ulrich, 2002; Vaidya and Johnston, 2013). 532 To test whether in human supragranular pyramidal neurons I<sub>h</sub> also promotes the 533 selective transfer of frequencies in the theta frequency range, we initiated AMPA-534 like synaptic input with a Poisson process (4 Hz) at 1000 locations along the 535 dendritic arbor (Figure 7H-inset). Comparing the  $I_h(+)$  and  $I_h(-)$  models revealed 536 that the presence of  $I_{\rm h}$  resulted in an increase in power in the 5-15 Hz range of 537 the somatic voltage response (Figure 7H). Thus, although the dendrite was 538 presented with a random spatial-temporal pattern of input, frequencies in the 5-539 15 Hz range were preferably passed to the soma in the  $I_{h}(+)$  model. The high 540 pass filtering properties of I<sub>h</sub> together with the low pass filtering properties of the 541 passive dendritic membrane impart the band pass shape of this transfer function 542 (Hutcheon and Yarom, 2000).

543

544

545

# **Discussion**

547	We have provided new evidence indicating a disparate contribution of h-
548	channels to human versus mouse supragranular pyramidal neuron properties.
549	In contrast to mouse, human supragranular excitatory neurons ubiquitously
550	expressed HCN1 transcripts as well as transcripts for PEX5L, a gene coding for
551	an important regulatory protein of h-channel function. Consistent with this
552	observation, we observed more pronounced $I_h\text{-}related$ membrane properties in
553	human compared with mouse pyramidal neurons at all distances from the pial
554	surface, as well as depth-dependent differences in $R_{N}$ and excitability.
555	Furthermore, the h-channel blocker, ZD7288, affected these intrinsic membrane
556	properties in human more so than in mouse supragranular pyramidal neurons.
557	Finally, we used a computational model to provide evidence that the expression
558	of h-channels in human supragranular pyramidal neurons narrows the window for
559	synaptic integration by accelerating EPSP kinetics and promotes the transfer of
560	synaptic input containing theta frequencies from the dendrite to soma.
561	Previous studies have largely focused on differences in the morphological,
562	synaptic and/or passive membrane properties of rodent versus human
563	supragranular pyramidal neurons. For example, human neurons are larger and
564	possess a more complex dendritic arbor compared with mouse (Deitcher et al.,
565	2017; Mohan et al., 2015). Differences in dendritic morphology and passive
566	dendritic membrane properties could contribute to differences in the cable
567	properties of human versus rodent pyramidal neurons (Eyal et al., 2016).
568	Likewise, these differences, together with differences in synaptic properties may

569 contribute to the reported high bandwidth processing capabilities of human 570 neurons compared with mouse (Eyal et al., 2014; Testa-Silva et al., 2014). Our 571 observation of cortical depth-dependent differences in mouse versus human 572 pyramidal neuron properties adds to this growing list of interspecies disparities in 573 cortical pyramidal neuron properties. Intriguingly, the depth-dependent 574 differences in intrinsic properties we observe in human cortex parallel the 575 lamination and differentiation of cell size that occurs along the radial axis of the 576 supragranular layers (von Economo and Koskinas, 2007; Hill and Walsh, 2005; 577 Molnár et al., 2014; Rakic, 2009). As such, the depth-dependence of these 578 membrane properties may reflect an evolutionary adaptation for the expanded 579 supragranular cortex of humans.

580 Our findings contrast with a previous report that found few correlations 581 between L2/3 membrane properties and somatic depth from the pial surface in 582 human cortex (Deitcher et al., 2017). This discrepancy may be due to 583 differences in sampling. The dataset included in the previous report was smaller 584 than the current set (n = 25 versus n = 55). Thus, it is possible that our data set 585 captured more depth-dependent variability in intrinsic properties simply because 586 of increased sampling. Relatedly, we sampled a wider range of somatic depths 587 from the pial surface than the previous study (350-1600  $\mu$ m in the current study; 588 471-1192  $\mu$ m in the previous study). L2 begins ~275  $\mu$ m from the pial surface 589 and is  $\sim$  150 µm wide in human temporal cortex (von Economo and Koskinas, 590 2007). Similarly, deep L3 can extend up to 1600 µm from the pial surface in 591 temporal cortex (von Economo and Koskinas, 2007). Thus, the previous study

may not have sampled the most superficial of L2 or the deepest portions of L3,

593 where the largest differences in intrinsic membrane properties exist.

594 To our knowledge our findings are the first to directly implicate a particular 595 ion channel in differences between human and rodent pyramidal neuron 596 properties. Supragranular pyramidal neurons in rodent cortex express little h-597 channel-related protein or RNA (Figure 1; Lörincz et al., 2002; Santoro et al., 598 2000; Zeng et al., 2012). Furthermore, mouse and rat supragranular pyramidal 599 neurons display very few hallmarks of  $I_h$  (e.g. sag) across several areas of cortex 600 (Larkum et al., 2007; Routh et al., 2017; van Aerde and Feldmeyer, 2013). 601 Together, these observations suggest that  $I_{h}$  contributes very little to rodent 602 supragranular pyramidal neuron physiology regardless of cortical region. In 603 contrast, human supragranular pyramidal neurons display prominent voltage sag 604 (Deitcher et al., 2017; Foehring and Waters, 1991) that we show here is 605 dependent upon h-channels. Furthermore, sag and other I<sub>b</sub>-related properties in 606 human cortex are more prominent in deep, compared to superficial, L2/3 607 pyramidal neurons. We note, however, that  $I_h$  is unlikely to explain all of the 608 depth-dependent differences in intrinsic properties we observed between mouse 609 and human pyramidal neurons. Clearly other factors, including in morphology 610 and/or differential expression of conductances other than  $I_h$  may contribute to the 611 depth- and species-dependent differences in excitability, R<sub>N</sub> and subthreshold 612 filtering we observed.

613 Our findings have a few limitations and caveats that are inherent to 614 studying human brain tissue at this level of analysis. First, human physiology

- 616 may be influenced by neurological disease state. Notably, h-channels are
- 617 implicated in epilepsy (Brennan et al., 2016; Jung et al., 2007; Shin et al., 2008)
- and thus our results may be influenced by neuropathology. Several factors,
- 619 however, strengthen our conclusion that I<sub>h</sub> prominently contributes to the
- 620 membrane properties of human supragranular pyramidal neurons in the
- 621 neurotypical condition. First, the tissue obtained for these experiments was distal
- to the focus of the seizures and did not express overt signs of pathology.
- 623 Second, we found similarly prominent I<sub>h</sub>-related properties in 23 supragranular
- 624 pyramidal neurons of temporal cortex brain slices (Figure S4) derived from tumor
- 625 patients and in other cortical regions (Allen Cell Types data base -
- 626 http://celltypes.brain-map.org; Deitcher et al., 2017). Finally, h-channel subunit
- 627 RNA is abundant in pyramidal neurons in the supragranular layers of cortical
- 628 post-mortem tissue obtained from donor brains with no prior history of
- 629 neurological disorder (Figure 1; Zeng et al., 2012).
- 630 Functional implications

Deep L3 neurons possess the most prominent I<sub>h</sub>-related membrane properties in the supragranular layers of human temporal cortex. Deep L3 also corresponds to the sub-lamina containing the largest supragranular pyramidal neurons with the largest total dendritic length (von Economo and Koskinas, 2007; Mohan et al., 2015). Because of their large size, these neurons may require specialized intrinsic mechanisms to ensure faithful propagation of signals along their dendritic arbor. Our modeling results suggest that h-channels may serve inthis regard by counteracting capacitive filtering by the dendrite.

639 Our simulations also demonstrate that h-channels significantly affect the 640 integrative properties of human supragranular pyramidal neurons in a similar 641 manner as has been reported in rodent cortical L5 or hippocampal CA1 642 pyramidal neurons. (Dembrow et al., 2015; Vaidya and Johnston, 2013; Williams 643 and Stuart, 2000). Consistent with its role as a resonating conductance (Hu et al., 644 2002; Hutcheon and Yarom, 2000; Narayanan and Johnston, 2008), the 645 presence of  $I_h$  resulted in an increase in power in the theta (and higher) 646 frequency range (Figure 7H). The specific details of these effects will depend 647 upon several factors, including total abundance, subcellular localization and/or 648 gradients of the channels. In rodents, h-channels are enriched in the distal apical 649 dendrites of several types of pyramidal neurons in multiple brain regions (Harnett 650 et al., 2015; Kalmbach et al., 2013; Kole et al., 2006; Lörincz et al., 2002; 651 Williams and Stuart, 2000). Notably, we observed widespread expression in 652 human temporal cortex of a gene (PEX5L) that codes for Trip8b, a protein that is 653 necessary for dendritic enrichment of  $I_h$  (Lewis et al., 2009; 2011). Thus, our 654 results are consistent with the possibility that  $I_h$  is prominent in the dendrites of 655 human supragranular pyramidal neurons. Nevertheless, modeling studies 656 suggest that the effects of I<sub>h</sub> on EPSPs kinetics do not appear to depend on 657 subcellular gradients, but rather on total expression levels (Angelo et al., 2007; 658 Das and Narayanan, 2014). Thus, the effects of  $I_h$  we observed on synaptic

659	integration in c	our single neuror	model may r	not depend u	pon the exact

660 localization of h-channels, but rather, their total expression levels.

- 661 Finally, our results suggest that I<sub>h</sub> may significantly affect the spike
- 662 initiation dynamics of human supragranular pyramidal neurons. The presence of
- h-channels can switch the firing mode of a neuron from temporal integrator to
- 664 coincidence detector, whereby spiking is sensitive to correlated synaptic input
- rather than changes in mean presynaptic firing rate (Das and Narayanan, 2017;
- 666 2014; Ratté et al., 2013). For rodent neurons, there is an intimate relationship
- between sub- and suprathreshold spectral selectivity (Das and Narayanan, 2017;
- 668 2014). Thus, the spiking activity of human supragranular pyramidal neurons may
- be tuned to specific frequencies of synaptic input, and this selectivity may vary
- 670 with somatic depth from the pial surface. If so, the expression of h-channels in
- 671 supragranular pyramidal neurons may contribute to memory-related theta-
- 672 frequency phase-locking of single human neurons observed in vivo (Jacobs et
- 673 al., 2007; Rutishauser et al., 2010).

674

#### 675 Acknowledgments

676 We wish to thank the Allen Institute founder, Paul G. Allen, for his vision, 677 encouragement and support. We also wish to thank the Allen Institute for Brain 678 Science Tissue Procurement. Tissue Processing and Facilities teams for help in 679 coordinating the logistics of human tissue surgical tissue collection, transport and 680 processing. We also thank the Allen Institute for Brain Science Reagent 681 Preparation, Animal Care and In Vitro Single Cell Characterization teams. We 682 are grateful to our collaborators at the local hospital sites, including Tracie 683 Granger, Caryl Tongco, Matt Ormond, Jae-Guen Yoon, Nathan Hansen, Niki 684 Ellington, Rachel Iverson (Swedish Medical Center), Carolyn Bea, Gina DeNoble 685 and Allison Beller (Harborview Medical Center). We thank Dirk C. Keene at 686 Harborview/UW for consultation and support. We also thank Meanhwan Kim for 687 helpful discussions and suggestions. 688

689

690

691 **Figure Legends** 

# 692 Figure 1- *HCN1-4* RNA expression in human versus mouse neocortex. A)

693 Single nucleus HCN channel subunit mRNA expression in excitatory neurons

- 694 from human temporal cortex arranged by layer. Violin plots represent distribution
- of mRNA expression on a log scale with a maximum reads per kilobase per
- 696 million mapped reads (RPKM) value of 4000. For reference, single nucleus
- 697 HCN channel subunit mRNA expression in inhibitory neurons across all layers is
- also shown. There are approximately equal levels of *HCN1* expression in
- 699 excitatory neurons across the cortical layers. **B)** Single cell HCN channel subunit
- 700 mRNA expression in excitatory neurons from mouse visual cortex arranged by
- 701 layer. Violin plots represent distribution of mRNA expression on a log scale with a
- 702 maximum RPKM value of 400, ten times lower than for human cells. Lower levels
- of h-channel-related gene expression were observed in excitatory neurons in the
- supragranular compared with infragranular layers of mouse primary visual cortex.
- Robust *HCN1* expression was also observed in inhibitory neurons. **C)** ISH of
- 706 HCN1 in human temporal cortex at low magnification (left column, with near
- adjacent Nissl stained section for layer identification) and high magnification in
- deep L3. D) ISH of *HCN1* in mouse neocortex at low magnification (left column,
- with near adjacent Nissl stained section) and high magnification of TeA.

710

#### 711 Figure 2 - Human and mouse supragranular pyramidal neurons display 712 different subthreshold membrane properties. Example voltage sweeps 713 obtained from a superficial and deep supragranular pyramidal neuron in 714 response to a family of hyperpolarizing and depolarizing current injections in A) 715 mouse temporal association area and B) human middle temporal gyrus. C) In 716 mouse cortex, resting membrane potential and input resistance increase as a 717 function of somatic distance from pia. **D**) In the supragranular layers of human 718 middle temporal gyrus resting potential increases, but input resistance decreases 719 as function of somatic distance from pia. Arrows correspond to sample voltage 720 sweeps in A & B E) Resting potential and input resistance in mouse versus 721 human cortex as a function of normalized somatic position in supragranular 722 cortex. F) Data were also binned into four groups based on the normalized 723 distance of the soma from pia, where 1 is the most superficial quadrant and 4 is 724 the deepest. \* p < 0.0125, mouse versus human post-hoc t-test with Bonferroni 725 correction. 726 Figure 3 – I<sub>h</sub>-related membrane properties are more pronounced in human 727 compared with mouse supragranular pyramidal neurons A) Example voltage 728 sweeps were obtained from current injections that yielded ~ 6 mV

hyperpolarization in **A**) mouse and **B**) human supragranular pyramidal neurons.

Arrows denote voltage sag and rebound potentials associated with the presence

731 of  $I_h$ . C) Mouse neurons display little voltage sag or rebound from

hyperpolarization in response to hyperpolarizing current injections. D) In contrast,

rebound and sag were prominent in human supragranular cortex, especially in

deep layer 3. Arrows correspond to sample voltage sweeps in A & B. E) Sag and

rebound in mouse and human cortex as a function of normalized somatic position

in supragranular cortex. F) As before, data were also binned into four groups. \*

737 p < 0.001 mixed factor ANOVA effect of species.

738

#### 739 Figure 4 - Mouse and human supragranular pyramidal neurons display

740 **different subthreshold filtering properties.** Example voltage responses to a

chirp stimulus current injection in a superficial and deep supragranular pyramidal

neuron in **A**) mouse and **B**) human cortex. ZAP and normalized frequency

response curves are also shown for these example neurons. Dotted lines mark

the resonant frequency in the ZAP and the 3dB cutoff in the normalized

frequency response curves. C) Mouse neurons were largely non-resonant

regardless of their position within supragranular cortex and became more low-

pass as a function of somatic depth from pia. **D)** Resonant frequency correlated

with somatic depth from pia in human cortex. Additionally, in human cortex, 3dB

cutoff frequency was correlated with somatic depth from pia. Arrows correspond

to sample voltage sweeps in A & B. E) Resonant frequency and 3dB cutoff as a

function of normalized depth from pia in mouse and human supragranular cortex.

**D)** Data binned into quadrants. For binned resonant frequency data \* p < 0.001

mixed factor ANOVA effect of species. For binned 3 dB cutoff data \* p < 0.0125,

mouse versus human post-hoc t-test with Bonferroni correction.

755

#### 756 Figure 5 - Excitability of mouse versus human pyramidal neurons as a

757 function of somatic distance from pia. A) The number of APs elicited by a 758 given current injection increased as a function of somatic depth from pia in 759 supragranular mouse cortex. Example sweeps obtained from a superficial and 760 deep neuron in response to 250, 500 and 750 pA are shown. B) The number of 761 APs elicited by a given current injection decreased as a function of somatic depth 762 from pia in supragranular human cortex. Example sweeps obtained from a 763 superficial and deep neuron in response to 250, 500 and 750 pA are shown. 764 Arrows correspond to sample voltage sweeps in A & B. C) Average firing rate as 765 a function of normalized position within supragranular cortex in mouse versus 766 human. **D)** Average firing rate of mouse and human supragranular pyramidal 767 neurons binned by somatic depth from pia. \* < 0.0125 mouse versus human 768 post-hoc t-test with Bonferroni correction.

769

#### 770 Figure 6 - Pharmacological evidence for I<sub>h</sub> in human supragranular

771 pyramidal neurons. A) Bath application of 10 µM ZD7288 produced a ~10 mV 772 hyperpolarization of the resting membrane potential in human neurons, but no 773 consistent change in mouse neurons. The plot at the left shows resting 774 membrane potential as a function of time for two example recordings. B) 10 µM 775 ZD7288 had a larger effect on the input resistance of human compared with 776 mouse supragranular pyramidal neurons. Example voltage responses to 777 hyperpolarizing current injections are shown to the left. C) Bath application of 10 778  $\mu$ M ZD7288 increased the number of action potentials produced by a given

- current injection in human pyramidal neurons, but not mouse pyramidal neurons.
- 780 Plots are averages from 6 human and 5 mouse experiments. Voltage responses
- are from example experiments.
- 782

#### **Figure 7** –I<sub>h</sub> affects the subthreshold integrative properties of a

#### morphologically precise human L3 pyramidal neuron model.

- A) Intracellular somatic chirp stimulation produced a subthreshold somatic
- voltage response in a L3 pyramidal neuron (green). The identical stimulation
- protocol was imposed on a biophysically detailed model that includes  $(I_h(+); red)$
- or excludes (I<sub>h</sub>(-); blue) I<sub>h</sub>. **B**) Power spectrum of somatic membrane potential
- response to intracellular chirp stimulation shown in panel A (blue: experiment;
- green:  $I_h(+)$  model; red:  $I_h(-)$  model). In both the  $I_h(+)$  model and the experiment,
- the frequency response curves are nearly overlapping with a resonant peak at ~
- 5 Hz. C) Morphological reconstruction of a human L3 pyramidal neuron used for
- the simulations shown here **D**) Single (left) or bursts (right) of AMPA-like
- conductances were injected at single synaptic locations (top) and the resultant
- 795 local dendritic and propagated somatic voltage response were recorded in the
- $I_h(+)$  (blue) and the  $I_h(-)$  model (red). The locations of 12 separate synaptic inputs
- are shown in panel C). E) The delay between the maximal amplitude of AMPA-
- 798 like conductance and EPSPs peak recorded at the soma as a function of
- synaptic distance from soma in the  $I_h(+)$  (blue) and the  $I_h(-)$  model. **F)** Synaptic
- 800 delays and half-width of the EPSPs calculated for lh(+) and lh(-) models. G) The
- 801 integral of EPSPs recorded at the soma in response to bursts of synaptic input at

- 802 various frequencies. The somatic response in the  $I_h(+)$  model was decreased
- relative to the  $I_h(-)$  model across several frequencies of synaptic input. **H**) –
- 804 Power spectrum of the somatic membrane potential of the  $I_h(+)$  and  $I_h(-)$  model
- 805 when stimulated by 1000 synapses randomly located along the apical dendrite
- 806 (synaptic conductance: 0.001 mS/cm<sup>2</sup>; morphology same as in panel C). Black
- 807 stripes at 1 correspond to statistically significant differences in the power
- 808 spectrum (2 sample Kolmogorov-Smirnov test; p<0.01). Inset: location of a
- subset (100 out of 1000) synapses is shown.
- 810

#### 811 **References**

- Allen Institute for Brain Science, 2016. Allen Cell Types Database Technical
  White Paper: Electrophysiology [WWW Document]. help.brain-map.org. URL
  http://help.brain-map.org/download/attachments/8323525/MorphOverview.pdf
  (accessed 2.28.18).
- Andrasfalvy, B.K., Magee, J.C., 2001. Distance-dependent increase in AMPA
   receptor number in the dendrites of adult hippocampal CA1 pyramidal
   neurons. Journal of Neuroscience 21, 9151–9159.
- Angelo, K., London, M., Christensen, S.R., Hausser, M., 2007. Local and Global
  Effects of Ih Distribution in Dendrites of Mammalian Neurons. Journal of
  Neuroscience 27, 8643–8653. doi:10.1523/JNEUROSCI.5284-06.2007
- Angevine, J.B., Sidman, R.L., 1961. Autoradiographic study of cell migration during histogenesis of cerebral cortex in the mouse. Nature 192, 766–768.
- Bean, B.P., 2007. The action potential in mammalian central neurons. Nat Rev
   Neurosci 8, 451–465. doi:10.1038/nrn2148
- Brager, D.H., Johnston, D., 2007. Plasticity of intrinsic excitability during longterm depression is mediated through mGluR-dependent changes in I(h) in
  hippocampal CA1 pyramidal neurons. Journal of Neuroscience 27, 13926–
  13937. doi:10.1523/JNEUROSCI.3520-07.2007
- Brennan, G.P., Baram, T.Z., Poolos, N.P., 2016. Hyperpolarization-Activated
  Cyclic Nucleotide-Gated (HCN) Channels in Epilepsy. Cold Spring Harb
  Perspect Med 6, a022384. doi:10.1101/cshperspect.a022384
- Cook, E.P., Guest, J.A., Liang, Y., Masse, N.Y., Colbert, C.M., 2007. Dendrite-tosoma input/output function of continuous time-varying signals in hippocampal
  CA1 pyramidal neurons. J. Neurophysiol. 98, 2943–2955.
  doi:10.1152/ip.00414.2007
- 836 doi:10.1152/jn.00414.2007

## B37 Das, A., Narayanan, R., 2017. Theta-frequency selectivity in the somatic spike-

triggered average of rat hippocampal pyramidal neurons is dependent on

839	HCN channels. J. Neurophysiol. 118, 2251–2266.
840	doi:10.1523/ENEURO.0001-16.2016
841	Das, A., Narayanan, R., 2014. Active dendrites regulate spectral selectivity in
842	location-dependent spike initiation dynamics of hippocampal model neurons.
843	Journal of Neuroscience 34, 1195–1211. doi:10.1523/JNEUROSCI.3203-
844	13.2014
845	DeFelipe, J., 2011. The evolution of the brain, the human nature of cortical
846	circuits, and intellectual creativity 1–17.
847	doi:10.3389/fnana.2011.00029/abstract
848	Deitcher, Y., Eyal, G., Kanari, L., Verhoog, M.B., Atenekeng Kahou, G.A.,
849	Mansvelder, H.D., de Kock, C.P.J., Segev, I., 2017. Comprehensive Morpho-
850	Electrotonic Analysis Shows 2 Distinct Classes of L2 and L3 Pyramidal
851	Neurons in Human Temporal Cortex. Cerebral Cortex 1–17.
852	doi:10.1093/cercor/bhx226
853	Dembrow, N.C., Chitwood, R.A., Johnston, D., 2010. Projection-specific
854	neuromodulation of medial prefrontal cortex neurons. Journal of
855	Neuroscience 30, 16922–16937. doi:10.1523/JNEUROSCI.3644-10.2010
856	Dembrow, N.C., Zemelman, B.V., Johnston, D., 2015. Temporal dynamics of L5
857	dendrites in medial prefrontal cortex regulate integration versus coincidence
858	
oso 859	detection of afferent inputs. Journal of Neuroscience 35, 4501–4514. doi:10.1523/JNEUROSCI.4673-14.2015
860	von Economo, C.F., Koskinas, G.N., 2007. Atlas of Cytoarchitectonics of the
861	Adult Human Cerebral Cortex. S. Karger AG (Switzerland).
862	Eyal, G., Mansvelder, H.D., de Kock, C.P.J., Segev, I., 2014. Dendrites Impact
863	the Encoding Capabilities of the Axon. Journal of Neuroscience 34, 8063–
864	8071. doi:10.1523/JNEUROSCI.5431-13.2014
865	Eyal, G., Verhoog, M.B., Testa-Silva, G., Deitcher, Y., Lodder, J.C., Benavides-
866	Piccione, R., Morales, J., DeFelipe, J., de Kock, C.P., Mansvelder, H.D.,
867	Segev, I., 2016. Unique membrane properties and enhanced signal
868	processing in human neocortical neurons. Elife 5. doi:10.7554/eLife.16553
869	Fan, Y., Fricker, D., Brager, D.H., Chen, X., Lu, HC., Chitwood, R.A., Johnston,
870	D., 2005. Activity-dependent decrease of excitability in rat hippocampal
871	neurons through increases in Ih. Nature Neuroscience 8, 1542–1551.
872	doi:10.1038/nn1568
873	Foehring, R.C., Waters, R.S., 1991. Contributions of low-threshold calcium
874	current and anomalous rectifier (Ih) to slow depolarizations underlying burst
875	firing in human neocortical neurons in vitro. Neuroscience Letters 124, 17–
876	21.
877	Gouwens, N.W., Berg, J., Feng, D., Sorensen, S.A., Zeng, H., Hawrylycz, M.J.,
878	Koch, C., Arkhipov, A., 2018. Systematic generation of biophysically detailed
879	models for diverse cortical neuron types. Nat Commun 1–13.
880	doi:10.1038/s41467-017-02718-3
881	Gu, N., Vervaeke, K., Hu, H., Storm, J.F., 2005. Kv7/KCNQ/M and HCN/h, but
882	not KCa2/SK channels, contribute to the somatic medium after-
883	hyperpolarization and excitability control in CA1 hippocampal pyramidal cells.
884	The Journal of Physiology 566, 689–715. doi:10.1113/jphysiol.2005.086835

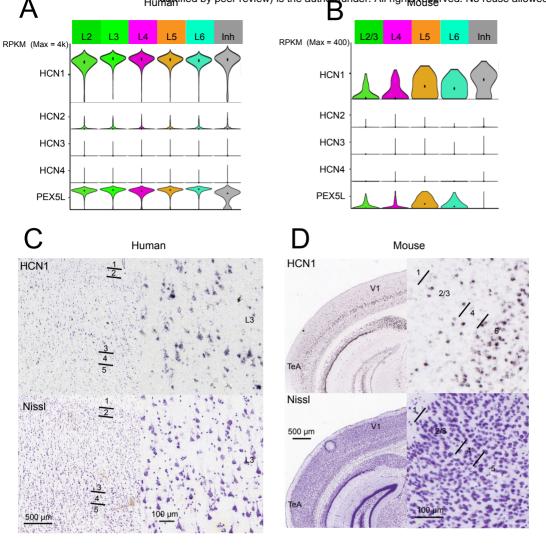
885 Harnett, M.T., Magee, J.C., Williams, S.R., 2015. Distribution and Function of 886 HCN Channels in the Apical Dendritic Tuft of Neocortical Pyramidal Neurons. 887 J. Neurosci. 35, 1024–1037. doi:10.1523/JNEUROSCI.2813-14.2015 888 Hill, R.S., Walsh, C.A., 2005. Molecular insights into human brain evolution. 889 Nature 437, 64–67. doi:10.1038/nature04103 890 Hu, H., Vervaeke, K., Storm, J.F., 2002. Two forms of electrical resonance at 891 theta frequencies, generated by M-current, h-current and persistent Na+ 892 current in rat hippocampal pyramidal cells. The Journal of Physiology 545, 893 783-805. 894 Hutcheon, B., Miura, R.M., Puil, E., 1996. Subthreshold membrane resonance in 895 neocortical neurons. J. Neurophysiol. 76, 683-697. 896 Hutcheon, B., yarom, Y., 2000. Resonance, oscillation and the intrinsic frequency 897 preferences of neurons. Trends in Neurosciences 23, 216–222. 898 Jacobs, J., Kahana, M.J., Ekstrom, A.D., Fried, I., 2007. Brain Oscillations 899 Control Timing of Single-Neuron Activity in Humans. Journal of Neuroscience 900 27, 3839–3844. doi:10.1523/JNEUROSCI.4636-06.2007 901 Johnston, D., Narayanan, R., 2008. Active dendrites: colorful wings of the 902 mysterious butterflies. Trends in Neurosciences 31, 309-316. 903 doi:10.1016/i.tins.2008.03.004 904 Jonas, P., Sakmann, B., 1992. Glutamate receptor channels in isolated patches 905 from CA1 and CA3 pyramidal cells of rat hippocampal slices. The Journal of 906 Physiology 455, 143-171. 907 Jung, S., Jones, T.D., Lugo, J.N., Sheerin, A.H., Miller, J.W., D'Ambrosio, R., 908 Anderson, A.E., Poolos, N.P., 2007. Progressive Dendritic HCN 909 Channelopathy during Epileptogenesis in the Rat Pilocarpine Model of 910 Epilepsy. J. Neurosci. 27, 13012–13021. doi:10.1523/JNEUROSCI.3605-911 07.2007 912 Kalmbach, B.E., Chitwood, R.A., Dembrow, N.C., Johnston, D., 2013. Dendritic 913 generation of mGluR-mediated slow afterdepolarization in layer 5 neurons of 914 prefrontal cortex. Journal of Neuroscience 33, 13518-13532. 915 doi:10.1523/JNEUROSCI.2018-13.2013 916 Kalmbach, B.E., Gray, R., Johnston, D., Cook, E.P., 2017. Systems-based 917 analysis of dendritic nonlinearities reveals temporal feature extraction in 918 mouse L5 cortical neurons. J. Neurophysiol. 117, 2188-2208. 919 doi:10.1152/jn.00951.2016 920 Kalmbach, B.E., Johnston, D., Brager, D.H., 2015. Cell-Type Specific 921 Channelopathies in the Prefrontal Cortex of the fmr1-/y Mouse Model of 922 Fragile X Syndrome(1.2.3). eNeuro 2. doi:10.1523/ENEURO.0114-15.2015 923 Koch, C., 2004. Biophysics of Computation. Oxford University Press. 924 Koch, C., 1984. Cable theory in neurons with active, linearized membranes. Biol 925 Cybern 50, 15–33. 926 Koch, C., Douglas, R., Wehmeier, U., 1990. Visibility of synaptically induced 927 conductance changes: theory and simulations of anatomically characterized 928 cortical pyramidal cells. J. Neurosci. 10, 1728–1744. 929 Kole, M.H.P., Hallermann, S., Stuart, G.J., 2006. Single Ih channels in pyramidal 930 neuron dendrites: properties, distribution, and impact on action potential

931 output. Journal of Neuroscience 26, 1677-1687. 932 doi:10.1523/JNEUROSCI.3664-05.2006 933 Larkum, M.E., Waters, J., Sakmann, B., Helmchen, F., 2007. Dendritic Spikes in 934 Apical Dendrites of Neocortical Layer 2/3 Pyramidal Neurons. J. Neurosci. 27, 8999–9008. doi:10.1523/JNEUROSCI.1717-07.2007 935 936 Lewis, A.S., Schwartz, E., Savio Chan, C., Noam, Y., Shin, M., Wadman, W.J., 937 James Surmeier, D., Baram, T.Z., Macdonald, R.L., Chetkovich, D.M., 2009. 938 Alternatively Spliced Isoforms of TRIP8b Differentially Control h Channel 939 Trafficking and Function. Journal of Neuroscience 29, 6250–6265. 940 doi:10.1523/JNEUROSCI.0856-09.2009 941 Lewis, A.S., Vaidya, S.P., Blaiss, C.A., Liu, Z., Stoub, T.R., Brager, D.H., Chen, 942 X., Bender, R.A., Estep, C.M., Popov, A.B., Kang, C.E., Van Veldhoven, P.P., 943 Bayliss, D.A., Nicholson, D.A., Powell, C.M., Johnston, D., Chetkovich, D.M., 944 2011. Deletion of the Hyperpolarization-Activated Cyclic Nucleotide-Gated 945 Channel Auxiliary Subunit TRIP8b Impairs Hippocampal Ih Localization and 946 Function and Promotes Antidepressant Behavior in Mice. J. Neurosci. 31, 947 7424-7440. doi:10.1523/JNEUROSCI.0936-11.2011 948 Lörincz, A., Notomi, T., Tamás, G., Shigemoto, R., Nusser, Z., 2002. Polarized 949 and compartment-dependent distribution of HCN1 in pyramidal cell dendrites. 950 Nature Neuroscience 5, 1185–1193. doi:10.1038/nn962 951 Magee, J., 1999. Dendritic Ih normalizes temporal summation in hippocampal 952 CA1 neurons. Nature Neuroscience 2, 848. doi:10.1038/12229 953 Magee, J.C., 1998. Dendritic hyperpolarization-activated currents modify the 954 integrative properties of hippocampal CA1 pyramidal neurons. J. Neurosci. 955 18, 7613-7624. 956 Magee, J.C., Cook, E.P., 2000. Somatic EPSP amplitude is independent of 957 synapse location in hippocampal pyramidal neurons. Nature Neuroscience 3, 958 895-903. doi:10.1038/78800 959 Mauro, A., 1961. Anomalous impedance, a phenomenological property of time-960 variant resistance. An analytic review. Biophys. J. 1, 353-372. 961 Mohan, H., Verhoog, M.B., Doreswamy, K.K., Eyal, G., Aardse, R., Lodder, B.N., 962 Goriounova, N.A., Asamoah, B., B Brakspear, A.B.C., Groot, C., van der 963 Sluis, S., Testa-Silva, G., Obermayer, J., Boudewijns, Z.S.R.M., Narayanan, 964 R.T., Baaven, J.C., Segev, I., Mansvelder, H.D., de Kock, C.P.J., 2015. 965 Dendritic and Axonal Architecture of Individual Pyramidal Neurons across 966 Lavers of Adult Human Neocortex. Cerebral Cortex 25, 4839–4853. 967 doi:10.1093/cercor/bhv188 968 Molnár, Z., Kaas, J.H., de Carlos, J.A., Hevner, R.F., Lein, E., Němec, P., 2014. 969 Evolution and development of the mammalian cerebral cortex. Brain Behav. 970 Evol. 83. 126-139. doi:10.1159/000357753 971 Naravanan, R., Johnston, D., 2008. The h Channel Mediates Location 972 Dependence and Plasticity of Intrinsic Phase Response in Rat Hippocampal 973 Neurons. J. Neurosci. 28, 5846–5860. doi:10.1523/JNEUROSCI.0835-974 08.2008 975 Narayanan, R., Johnston, D., 2007. Long-Term Potentiation in Rat Hippocampal 976 Neurons Is Accompanied by Spatially Widespread Changes in Intrinsic

977	Oscillatory Dynamics and Excitability. Neuron 56, 1061–1075.
978	doi:10.1016/j.neuron.2007.10.033
979	Nolan, M.F., Malleret, G., Dudman, J.T., Buhl, D.L., Santoro, B., Gibbs, E.,
980	Vronskaya, S., Buzsáki, G., Siegelbaum, S.A., Kandel, E.R., Morozov, A.,
981	2004. A Behavioral Role for Dendritic Integration. Cell 119, 719–732.
982	doi:10.1016/j.cell.2004.11.020
983	Peng, H., Ruan, Z., Long, F., Simpson, J.H., Myers, E.W., 2010. V3D enables
984	real-time 3D visualization and quantitative analysis of large-scale biological
985	image data sets. Nature Biotechnology 28, 348–353. doi:10.1038/nbt.1612
986	Rakic, P., 2009. Evolution of the neocortex: a perspective from developmental
987	biology. Nat Rev Neurosci 10, 724–735. doi:10.1038/nrn2719
988	Rakic, P., 1974. Neurons in rhesus monkey visual cortex: systematic relation
989	between time of origin and eventual disposition. Science 183, 425–427.
990	Rall, W., 1967. Distinguishing theoretical synaptic potentials computed for
991	different soma-dendritic distributions of synaptic input. J. Neurophysiol. 30,
992	1138–1168. doi:10.1152/jn.1967.30.5.1138
993	Ratté, S., Hong, S., De Schutter, E., Prescott, S.A., 2013. Impact of neuronal
994	properties on network coding: roles of spike initiation dynamics and robust
995	synchrony transfer. Neuron 78, 758–772. doi:10.1016/j.neuron.2013.05.030
996	Reyes, A., 2001. Influence of dendritic conductances on the input-output
997	properties of neurons. Annu. Rev. Neurosci. 24, 653–675.
998	doi:10.1146/annurev.neuro.24.1.653
999	Robinson, R.B., Siegelbaum, S.A., 2003. Hyperpolarization-activated cationic
1000	currents: From Molecules to Physiological Function. Annu. Rev. Physiol. 65,
1001	453–480. doi:10.1146/annurev.physiol.65.092101.142734
1002	Routh, B.N., Rathour, R.K., Baumgardner, M.E., Kalmbach, B.E., Johnston, D.,
1003	Brager, D.H., 2017. Increased transient Na +conductance and action
1004	potential output in layer 2/3 prefrontal cortex neurons of the fmr1 -/ymouse.
1005	The Journal of Physiology 595, 4431–4448. doi:10.1083/jcb.143.5.1295
1006	Rutishauser, U., Ross, I.B., Mamelak, A.N., Schuman, E.M., 2010. Human
1007	memory strength is predicted by theta-frequency phase-locking of single
1008	neurons. Nature 464, 903–907. doi:10.1038/nature08860
1009	Santoro, B., 2004. Regulation of HCN Channel Surface Expression by a Novel C-
1010	Terminal Protein-Protein Interaction. Journal of Neuroscience 24, 10750–
1011	10762. doi:10.1523/JNEUROSCI.3300-04.2004
1012	Santoro, B., Chen, S., Luthi, A., Pavlidis, P., Shumyatsky, G.P., Tibbs, G.R.,
1013	Siegelbaum, S.A., 2000. Molecular and functional heterogeneity of
1014	hyperpolarization-activated pacemaker channels in the mouse CNS. J.
1015	Neurosci. 20, 5264–5275.
1016	Shin, M., Brager, D., Jaramillo, T.C., Johnston, D., Chetkovich, D.M., 2008.
1017	Mislocalization of h channel subunits underlies h channelopathy in temporal
1018	lobe epilepsy. Neurobiology of Disease 32, 26–36.
1019	doi:10.1016/j.nbd.2008.06.013
1020	Spruston, N., Jonas, P., Sakmann, B., 1995. Dendritic glutamate receptor
1021	channels in rat hippocampal CA3 and CA1 pyramidal neurons. The Journal of
1022	Physiology 482 ( Pt 2), 325–352.

- 1023 Stuart, G., Spruston, N., 1998. Determinants of voltage attenuation in neocortical 1024 pyramidal neuron dendrites. J. Neurosci. 18, 3501–3510.
- Stuart, G.J., Spruston, N., 2015. Dendritic integration: 60 years of progress.
   Nature Neuroscience 18, 1713–1721. doi:10.1038/nn.4157
- Tasic, B., Menon, V., Nguyen, T.N., Kim, T.K., Jarsky, T., Yao, Z., Levi, B., Gray,
  L.T., Sorensen, S.A., Dolbeare, T., Bertagnolli, D., Goldy, J., Shapovalova,
- 1029 N., Parry, S., Lee, C., Smith, K., Bernard, A., Madisen, L., Sunkin, S.M.,
- 1030 Hawrylycz, M., Koch, C., Zeng, H., 2016. Adult mouse cortical cell taxonomy 1031 revealed by single cell transcriptomics. Nature Neuroscience 19, 335–346.
- 1032 doi:10.1038/nn.4216
- 1033 Testa-Silva, G., 2010. Human synapses show a wide temporal window for spike-1034 timing-dependent plasticity. Front. Syn.Neurosci.
- 1035 doi:10.3389/fnsyn.2010.00012
- 1036 Testa-Silva, G., Verhoog, M.B., Linaro, D., de Kock, C.P.J., Baayen, J.C.,
- Meredith, R.M., De Zeeuw, C.I., Giugliano, M., Mansvelder, H.D., 2014. High
  Bandwidth Synaptic Communication and Frequency Tracking in Human
  Neocortex. PLoS Biol 12, e1002007. doi:10.1371/journal.pbio.1002007.s014
- Ting, J.T., Daigle, T.L., Chen, Q., Feng, G., 2014. Acute Brain Slice Methods for
   Adult and Aging Animals: Application of Targeted Patch Clamp Analysis and
   Optogenetics, in: Methods in Molecular Biology, Methods in Molecular
   Biology. Springer New York, New York, NY, pp. 221–242. doi:10.1007/978-1 4939-1096-0 14
- 1045 Ulrich, D., 2002. Dendritic resonance in rat neocortical pyramidal cells. J. 1046 Neurophysiol. 87, 2753–2759.
- 1047 Vaidya, S.P., Johnston, D., 2013. Temporal synchrony and gamma-to-theta
  1048 power conversion in the dendrites of CA1 pyramidal neurons. Nature
  1049 Neuroscience 16, 1812–1820. doi:10.1038/nn.3562
- 1050 van Aerde, K.I., Feldmeyer, D., 2013. Morphological and Physiological
  1051 Characterization of Pyramidal Neuron Subtypes in Rat Medial Prefrontal
  1052 Cortex. Cerebral Cortex 25, 788–805. doi:10.1093/cercor/bht278
- Wang, B., Yin, L., Zou, X., Ye, M., Liu, Y., He, T., Deng, S., Jiang, Y., Zheng, R.,
  Wang, Y., Yang, M., Lu, H., Wu, S., Shu, Y., 2015. A Subtype of Inhibitory
  Interneuron with Intrinsic Persistent Activity in Human and Monkey
- 1056 Neocortex. CellReports 10, 1450–1458. doi:10.1016/j.celrep.2015.02.018
   1057 Williams, S.R., Stuart, G.J., 2000. Site independence of EPSP time course is mediated by dendritic I(h) in neocortical pyramidal neurons. J. Neurophysiol.
- 1059 **83**, 3177–3182.
- 1060 Zeng, H., Shen, E.H., Hohmann, J.G., Oh, S.W., Bernard, A., Royall, J.J.,
- 1061 Glattfelder, K.J., Sunkin, S.M., Morris, J.A., Guillozet-Bongaarts, A.L., Smith,
- 1062 K.A., Ebbert, A.J., Swanson, B., Kuan, L., Page, D.T., Overly, C.C., Lein,
- 1063 E.S., Hawrylycz, M.J., Hof, P.R., Hyde, T.M., Kleinman, J.E., Jones, A.R.,
- 1064 2012. Large-Scale Cellular-Resolution Gene Profiling in Human Neocortex
- 1065 Reveals Species-Specific Molecular Signatures. Cell 149, 483–496.
- 1066 doi:10.1016/j.cell.2012.02.052
- 1067

bioRxiv preprint doi: https://doi.org/10.1101/312298; this version posted May 2, 2018. The copyright holder for this preprint ( Humanified by peer review) is the author/funder. All rights case rved. No reuse allowed without permission.



bioRxiv preprint doi: https://doi.org/10.1101/312298; this version posted May 2, 2018. The copyright holder for this preprint (v certified by peer review) is the author/funder. All rights reserved. No reuse allowed without permission.

